Dalton Transactions

ROYAL SOCIETY OF CHEMISTRY

COMMUNICATION

View Article Online
View Journal | View Issue

Cite this: *Dalton Trans.*, 2025, **54**, 11828

Received 9th June 2025,
Accepted 9th June 2025

DOI: 10.1039/d5dt01351h

rsc.li/dalton

Homocoupling of C_1 building blocks by a heterometallic Mg–Al complex†

Wenbang Yang, Andrew J. P. White and Mark R. Crimmin *

A heterometallic magnesium–aluminium hydride complex is reported for the selective homologation of C_1 building blocks (CO and CNXyl, Xyl = 2,6-$Me_2C_6H_3$) to form products containing C_2 and C_3 chains. CO reacts to form known deltate or ethynediolate motifs with different outcomes depending on the steric demands of the ligand on magnesium. In contrast, CNXyl reacts through a combination of carbon–carbon bond formation and hydride migration to form a novel metalated ethene diamidolate ligand $[RN^1C^1{=}C^2(H)N^2R]^{3-}$.

Carbon monoxide (CO), carbon dioxide (CO_2), and isocyanides (CNR, R = alkyl, aryl) have been extensively used as C_1-building blocks for the construction of more complex organic molecules.[1] For example, the Fischer–Tropsch (F–T) process combines CO and H_2 and can be viewed as a controlled polymerisation, hydrogenation, and deoxygenation of carbon monoxide.[2–4] Despite its impact, the F–T process suffers from low product selectivity forming both a distribution of carbon chain lengths and mixtures of alkanes, alkenes or oxygenates depending on the catalyst and precise conditions. In recent years, there has been growing interest in using C_1 building blocks to form atomically precise carbon chains.[5–8] The use of well-defined, homogenous, metal complexes has allowed identification of new selective chemical transformations. In particular, systems that contain two (or more) metal sites capable of synergistic binding and activation of C_1 building blocks have led to some remarkable examples of forming complex products with C_2–C_6 carbon chains and cycles.

For example, we previously showed that the aluminium(I) compound [{(Ar^1NCMe)$_2$CH}Al] (**1**, Ar^1 = 2,6-$iPr_2C_6H_3$) reacts with CO in the presence of transition metal carbonyl complexes to produce C_2, C_3 and C_4-chains (Scheme 1).[9–11] Similar reactions occur between **1** and CN(1-Ad) (1-Ad = 1-adamantyl), with addition of $[Mo(CO)_6]$ impacting the selectively of product formation.[12] The Jones group combined their low-oxidation state magnesium(I) complex [{(Ar^2NCMe)$_2$CH}Mg]$_2$ (Ar^2 = 2,4,6-$Me_3C_6H_2$ or 2,6-$Me_2C_6H_3$) with sub-stoichiometric amounts of $[Mo(CO)_6]$ to facilitate the cyclohexamerisation of CO to a benzene-hexolate moiety.[13] In the absence of $[Mo(CO)_6]$, related magnesium(I) species form either deltate or ethenediolate complexes, with the selectivity controlled by the sterics of the ligand on magnesium.[14–16] The magnesium hydride complexes [{(Ar^3NCMe)$_2$CH}MgH]$_2$ (**2a**, Ar^3 = 2,6-$iPr_2C_6H_3$; **2b**, Ar^3 = 2,6-EtC_6H_3) have also been shown to react with CO to generate *cis*-ethenediolate and cyclopropanetriolate complexes respectively.[17–19] Related magnesium alkyl complexes can promote the dimerisation and trimerisation of CO either through thermal or catalytic routes.[20–22] We have shown that tetrameric magnesium hydride clusters effect the coupling and deoxygenation of CO,[23] and the cross-coupling of CO and CNXyl.[24] In related studies, both anionic aluminium and magnesium complexes have been demonstrated to promote the coupling of either CO or CNR, achieving the formation of C_{2-6} chains.[25–30]

Despite the significant advances described above, there has been limited investigations into coupling reactions of CO (or isocyanides) mediated by complexes with heteronuclear metal–metal bonds. Herein we report the homologation of C_1 building blocks to C_2 and C_3 chains by reaction with an *in situ* generated heterometallic Mg–Al hydride complex.[31] We show that this heterometallic can participate in known reactivity to form deltate and ethynediolate motifs. But more importantly demonstrate a new mode of reactivity of an isocyanide that involves both carbon–carbon bond formation and hydride transfer to the carbon chain, generating a previously unknown trianionic ethene diamidolate fragment $[RNC{=}C(H)NR]^{3-}$ that bridges magnesium and aluminium centres. DFT calculations are used to probe the electronic structure of the metalated ethene diamidolate and rationalise the most likely mechanism for its formation.

Department of Chemistry, Molecular Sciences Research Hub, 82 Wood Lane, Shepherds Bush, London, W12 0BZ, UK. E-mail: m.crimmin@imperial.ac.uk

†Electronic supplementary information (ESI) available: Experimental procedures and details of calculations (PDF), crystallographic data for **4a**, **4b**, **5** and **6** (CIF) and computational coordinates (*XYZ*). CCDC 2363835–2363837 and 2425919. For ESI and crystallographic data in CIF or other electronic format see DOI: https://doi.org/10.1039/d5dt01351h

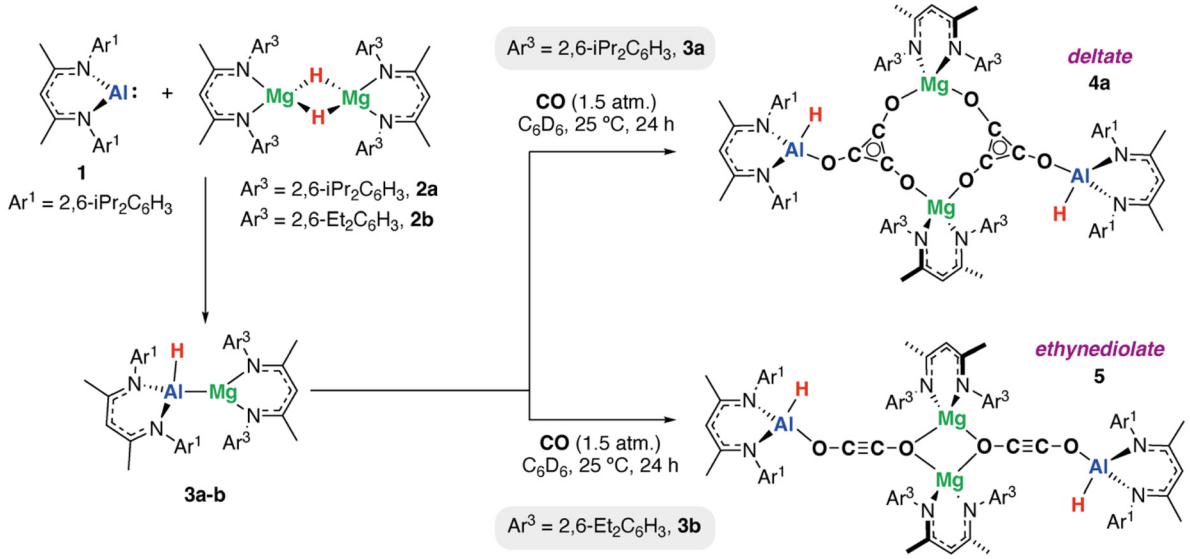

Scheme 1 Reactions of **3a** and **3b** CO to form deltate and ethynediolate complexes.

The reaction of **1** with the magnesium hydride complex **2a** was originally reported by Harder and co-workers,[31] and leads to the formation of the corresponding heterometallic Mg–Al hydride species **3a**. Herein we generated **3a**, and an analogue **3b**, *in situ* and reacted them directly with either CO or CNAr (Ar = 2,6-dimethylphenyl). Addition of excess CO to **3a** over 24 h at 25 °C in benzene-d_6 led to the formation of the deltate complex **4a** (Scheme 1). **4a** results from a threefold reaction of CO and incorporates both Mg and Al sites from the heterometallic precursor. In the solid state, **4a** contains a dimeric structure with two deltate ligands bridging magnesium sites. The ^{1}H and ^{13}C NMR spectroscopic data, are suggestive of a dynamic process which renders the three binding sites chemically and magnetically equivalent in solution. The hydride ligand remains unreacted and bound to aluminium appearing as a broad resonance at δ = 3.97 ppm in the ^{1}H NMR spectrum. **4a** crystallises alongside a minor byproduct **4b** derived from deprotonation and metalation of one the methyl groups of the β-diketiminate backbone (see ESI† for details). While the mechanism to form **4b** remains unclear, it can be readily separated from **4a** through fractional crystallisation in hexamethyldisiloxane.

The reaction outcome proved sensitive to the steric demands of the ligand on magnesium. Addition of CO to an *in situ* generated sample of **3b** over 24 h at 25 °C in benzene-d_6 led to the formation of the ethynediolate complex **5** (Scheme 1). **5** was characterised by diagnostic resonances at δ = 47.9 and 48.2 ppm in the ^{13}C NMR spectrum, consistent with an unsymmetrical ethynediolate moiety. In the solid-state, the C–C and C–O bond lengths of the deltate and ethynediolate fragments in **5a**, **5b**, and **6** are consistent with those reported previously (Fig. 1).[14,15]

Reaction of **3a** with 2,6-dimethylphenylisocyanide for 1 h at 25 °C in benzene-d_6 led to formation of **6** (Scheme 2). **6** contains a metalated ethene diamidolate ligand with a *trans*-geometry obtained by coupling of two isocyanides and hydride transfer from aluminium to carbon. This new C_2 fragment in **6** can be viewed as originating from a 2 : 1 reaction of CNXyl : hydride. This is the first time a simple metalated ethene diamidolate ligand, $[RN^1C^1{=}C^2(H)N^2R]^{3-}$, has been observed to form from reaction of an isocyanide and metal hydride complex. In C_6D_6 solution, **6** was characterised by a diagnostic proton of the ethene moiety H^1 which resonates at δ = 6.03 (s) ppm. This correlates with ^{13}C environments C^1 and C^2 at δ = 148.3 and 139.2 ppm respectively.

In the solid-state, **6** retains a heterometallic structure with a newly formed ethene diamidolate ligand which coordinates the Al atom through a κ^2-C^1,N^2 binding mode and the Mg atom through a κ^1-N^1 binding mode The $[RN^1C^1{=}C^2(H)N^2R]^{3-}$ moiety is formally a trianionic ligand. The Al–C^1 and Al–N^1 bonds lengths are 1.999(2) and 1.8514(19) Å respectively. The C^1–N^1, $C^1{=}C^2$, and C^2–N^2 bond lengths take values of 1.416(3), 1.354(3) and 1.453(3) Å respectively (Fig. 1).

DFT calculations were conducted to gain further insight into the electronic structure of the new $[RN^1C^1{=}C^2(H)N^2R]^{3-}$ motif in **6**, alongside its mechanism of formation from CNXyl and **3a**. Geometries were optimised with the B3PW91-D3 functional using a hybrid basis-set comprised of 6-311+G* (C,H,N, O) and SDDAll (Mg, Al). Solvation was considered using the polarizable continuum model (benzene). Single point corrections to energies were conducted with the 6-311+G** triple zeta basis-set.

NBO calculations on **6** suggest that the $[RN^1C^1{=}C^2(H)N^2R]^{3-}$ motif adopts a conjugated structure. The Wiberg Bond Indices (WBIs) take values of N^1–C^1 (1.16), $C^1{=}C^2$ (1.68) and C^2–N^2 (1.03). These data can be interpreted in terms of an alternating array of single and double bonds, however the N–C WBIs are slightly greater than expected for a single bond

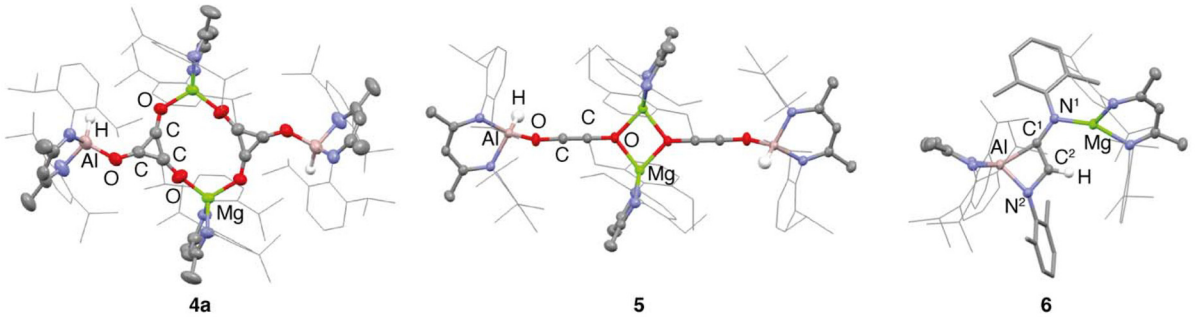

Fig. 1 Crystal Structures of **4a**, **5**, and **6**. Aryl groups on the β-diketiminate ligands are drawn as wireframe. Hydrogen atoms with the exception of hydride ligands have been omitted for clarity.

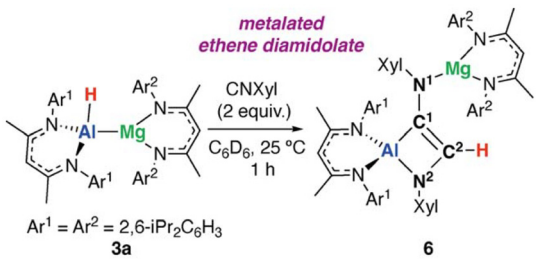

Scheme 2 Reaction of **3a** with CNXyl to form complex **6** which contains a metalated ethene diamidolate ligand.

suggesting a degree of delocalisation of the N lone-pair into the conjugated system. Binding to metals is primarily ionic with NPA charges on Al (+2.10) and Mg (+1.82) being highly positive and those on N^1 (−0.94), C^1 (−0.44), C^2 (−0.23) and N^2 (−0.99) uniformly negative. To further probe the electronic structure the parent non-coordinated trianion $[RN^1C^1{=}C^2(H)N^2R]^{3-}$ was calculated, this species shows a similar electronic structure to the coordinated fragment found in **6**, consistent with a large ionic contribution to the bonding to the metal sites.

Further calculations were undertaken to shed light on the mechanism that leads to the formation of **6** (Fig. 2). These calculations were initiated from **3a**. The lowest energy pathway identified is initiated from binding of CNXyl to the magnesium site of **3a** to form **Int-1**. This step is followed by the insertion of CNXyl into the Mg–Al bond *via* **TS-1** ($\Delta G^{\ddagger}_{298K}$ = 18.9 kcal mol^{-1}) and directly generates a dimetallated imine functional group in intermediate **Int-2**. The structure of **Int-2** is similar to the established intermediates reported in CO homologation.[15] **Int-2** can undergo a reorganisation into the thermodynamically more stable isomer **Int-3** by **TS-2** ($\Delta G^{\ddagger}_{298K}$ = 11.7 kcal mol^{-1}).

Subsequent coordination of another molecule of CNXyl to **Int-3** forms the intermediate **Int-4**. **Int-4** contains both adjacent imine and isocyanide ligands, which are suitably arranged

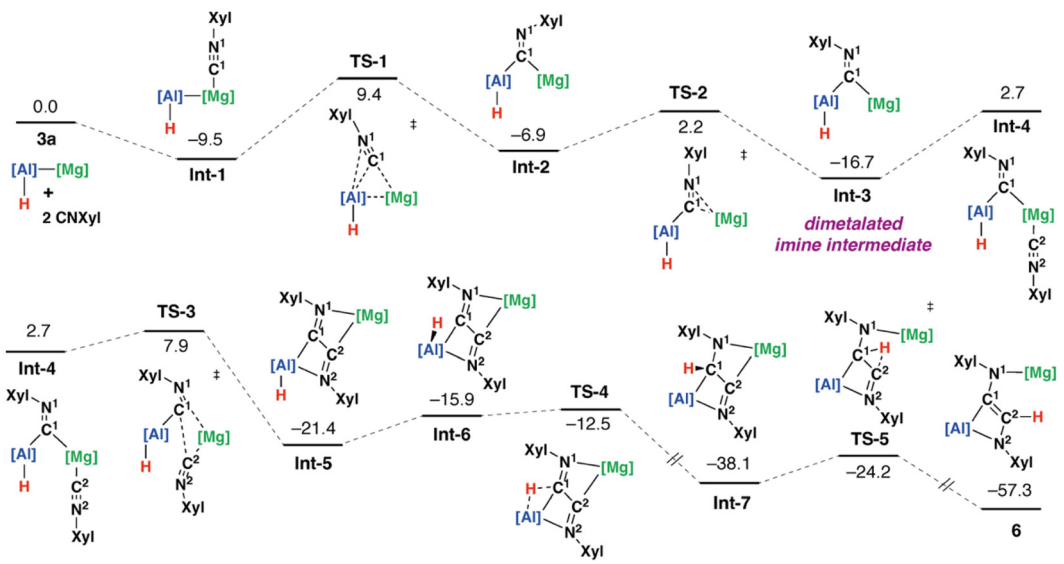

Fig. 2 Calculated pathway for the formation of **6** from **3a** and 2 equiv. of CNXyl. B3PW91-D3/6-311+G**/PCM (benzene)//B3PW91-D3/6-311+G*(C,H,N,O)/SDDAll (Mg)/PCM (benzene). Gibbs energies, values in kcal mol^{-1}.

for carbon–carbon bond formation. Nucleophilic attack of the metalated imine unit on the isocyanide group occurs *via* **TS-3** ($\Delta G^{\ddagger}_{298K}$ = 24.6 kcal mol^{-1}) to generate **Int-5**.[32,33] Along the potential energy surface from **Int-4** → **TS-3** → **Int-5** the Wiberg Bond Indices (WBIs) for the forming C^1–C^2 bond increase (0.13 → 0.45 → 1.07) while those for C^2–N^2 bond decrease (2.02 → 2.10 → 1.63). NPA charges are consistent with the imine carbon acting as the nucleophilic site with the charge on C^1 (−0.80 → −0.45 → 0.12) becoming more positive as the reaction progresses. Hydride transfer occurs through first a conformational change from **Int-5** to **Int-6**, followed by hydride migration to the C^1 position by **TS-4** ($\Delta G^{\ddagger}_{298K}$ = 8.9 kcal mol^{-1}) to form **Int-7**. Species related to **Int-5** and **Int-6** have been reported during the coupling of isonitriles with low-oxidation state magnesium complexes containing homonuclear Mg–Mg bonds.[34] A subsequent 1,2-migration from C^1 to C^2 *via* **TS-5** ($\Delta G^{\ddagger}_{298K}$ = 13.9 kcal mol^{-1}) ultimately affords the experimentally identified product **6**.

In summary, a heterometallic magnesium–aluminium hydride complex reacts with CO to form known C_2 and C_3 fragments namely ethynediolate and deltate ligands. Reaction with the isocyanide CNXyl (Xyl = 2,6-dimethylphenyl) leads instead to both C–C coupling and hydride transfer to form a new $[RN^1C^1{=}C^2(H)N^2R]^{3-}$ ligand. To our knowledge, this is the first example of homocoupling and reduction of an isocyanide to form such a fragment. DFT calculations support a mechanism for C–C bond formation through nucleophilic attack of a dimetallated imine functional group on a coordinated isocyanide. Our findings demonstrate that heterometallic complexes containing metal–metal bonds are suitable reagents to form carbon chains from CO and isocyanides. More importantly we demonstrate that these species give rise to new reactivity leading to selective formation of new products not yet observed with other main group or transition metal complexes.

Conflicts of interest

There are no conflicts to declare.

Data availability

Details of experimental procedures, characterisation data and computational modelling is provided in the ESI.†

Acknowledgements

The EPSRC is thanked for funding (EP/S036628/1).

References

1 A. Eschenmoser, *Tetrahedron*, 2007, **63**, 12821–12844.
2 A. Y. Khodakov, W. Chu and P. Fongarland, *Chem. Rev.*, 2007, **107**, 1692–1744.
3 M. E. Dry, *Catal. Today*, 2002, **71**, 227–241.
4 H. Schulz, *Appl. Catal., A*, 1999, **186**, 3–12.
5 S. Fujimori and S. Inoue, *J. Am. Chem. Soc.*, 2022, **144**, 2034–2050.
6 R. Y. Kong and M. R. Crimmin, *Dalton Trans.*, 2020, **49**, 16587–16597.
7 J. M. Parr and M. R. Crimmin, *Angew. Chem., Int. Ed.*, 2023, **62**, e202219203.
8 M. J. Evans and C. Jones, *Chem. Soc. Rev.*, 2024, **53**, 5054–5082.
9 R. Y. Kong, M. Batuecas and M. R. Crimmin, *Chem. Sci.*, 2021, **12**, 14845–14854.
10 R. Y. Kong and M. R. Crimmin, *J. Am. Chem. Soc.*, 2018, **140**, 13614–13617.
11 M. Batuecas, R. Y. Kong, A. J. P. White and M. R. Crimmin, *Angew. Chem., Int. Ed.*, 2022, **61**, e202202241.
12 C. Zhan, F. Dankert, Z. Jiang, B. Wang, D. Munz and J. Chu, *Angew. Chem., Int. Ed.*, 2023, **62**, e202307352.
13 A. Paparo, K. Yuvaraj, A. J. R. Matthews, I. Douair, L. Maron and C. Jones, *Angew. Chem., Int. Ed.*, 2021, **60**, 630–634.
14 K. Yuvaraj, I. Douair, D. D. L. Jones and C. Jones, *Chem. Sci.*, 2020, **11**, 3516–3522.
15 K. Yuvaraj, I. Douair, A. Paparo, L. Maron and C. Jones, *J. Am. Chem. Soc.*, 2019, **141**, 8764–8768.
16 K. Yuvaraj, J. C. Mullins, T. Rajeshkumar, I. Douair, L. Maron and C. Jones, *Chem. Sci.*, 2023, **14**, 5188–5195.
17 R. Lalrempuia, C. E. Kefalidis, S. J. Bonyhady, B. Schwarze, L. Maron, A. Stasch and C. Jones, *J. Am. Chem. Soc.*, 2015, **137**, 8944–8947.
18 M. D. Anker, M. S. Hill, J. P. Lowe and M. F. Mahon, *Angew. Chem., Int. Ed.*, 2015, **54**, 10009–10011.
19 M. D. Anker, C. E. Kefalidis, Y. Yang, J. Fang, M. S. Hill, M. F. Mahon and L. Maron, *J. Am. Chem. Soc.*, 2017, **139**, 10036–10054.
20 M. Wang, Y. Cai, T. Rajeshkumar, L. Maron and X. Xu, *Chem. – Eur. J.*, 2025, **31**, e202404594.
21 D. T. Nguyen, R. Mondal, M. J. Evans, J. M. Parr and C. Jones, *Angew. Chem., Int. Ed.*, 2025, e202500264.
22 K. Yuvaraj and C. Jones, *Chem. Commun.*, 2021, **57**, 9224–9227.
23 W. Yang, A. J. P. White and M. R. Crimmin, *Angew. Chem., Int. Ed.*, 2024, **63**, e202319626.
24 W. Yang, A. J. P. White and M. R. Crimmin, *Chem. Sci.*, 2024, **15**, 11807–11813.
25 M. J. Evans, M. D. Anker, C. L. McMullin and M. P. Coles, *Chem. Sci.*, 2023, **14**, 6278–6288.
26 M. J. Evans, M. G. Gardiner, M. D. Anker and M. P. Coles, *Chem. Commun.*, 2022, **58**, 5833–5836.
27 A. Heilmann, M. M. D. Roy, A. E. Crumpton, L. P. Griffin, J. Hicks, J. M. Goicoechea and S. Aldridge, *J. Am. Chem. Soc.*, 2022, **144**, 12942–12953.
28 H.-Y. Liu, R. J. Schwamm, S. E. Neale, M. S. Hill, C. L. McMullin and M. F. Mahon, *J. Am. Chem. Soc.*, 2021, **143**, 17851–17856.

29 A. O'Reilly, M. D. Haynes, C. L. McMullin, S. Harder, Z. R. Turner, D. O'Hare, J. R. Fulton and M. P. Coles, *Chem. Commun.*, 2024, **60**, 7204–7207.
30 M. J. Evans and C. Jones, *Inorg. Chem.*, 2023, **2023**, 14393–14401.
31 S. Brand, H. Elsen, J. Langer, S. Grams and S. Harder, *Angew. Chem., Int. Ed.*, 2019, **58**, 15496–15503.
32 W. Chen, Y. Zhao, W. Xu, J.-H. Su, L. Shen, L. Liu, B. Wu and X.-J. Yang, *Chem. Commun.*, 2019, **55**, 9452–9455.
33 W. Uhl, U. Schütz, W. Hiller and M. Heckel, *Chem. Ber.*, 1994, **127**, 1587–1592.
34 M. Ma, A. Stasch and C. Jones, *Chem. – Eur. J.*, 2012, **18**, 10669–10676.